An Electro thermal-Chemical Technology for Thermal Spray Coatings

S. Wald, G. Appelbaum, R. Alimi, L. Rabani, S. Cuperman, C. Bruma, D. Zoler, V. Zhitomirsky, M. Factor and I. Roman

1. Abstract

A new spray technology for producing hard-coatings, has been developed at the SOREQ Nuclear Research Center.

The concept is based on the extensive experience accumulated at SOREQ in the course of the development of Electrothermal (ET), Electrothermal-Chemical (ETC) and Solid-Propellant Electrothermal-Chemical (SPETC) guns[1].

High quality coatings may be obtained by thermal spraying powder particles onto a variety of substrates. Mature state-of-the-art technologies such as plasma spray, high velocity oxyfuel (HVOF) and detonation gun (D-Gun) are widely used for many applications. As each method has its own drawbacks there is a need for a combination of several parameters which cannot be achieved by any existing individual commercial technology. The method presented is oriented toward a high-quality, multi-step, high-throughput, easily programmable continuous coating process and relatively inexpensive technology.

The combustion products of a solid or liquid propellant accelerate the powder particles of the coating material. A pulsed-plasma jet, provided by a confined capillary discharge, ignites the propellant and controls the combustion process. The powder particles are accelerated to velocities over 1000 m/s. Due to the very high carrier gas density, high velocity, high throughput and high powder consumption efficiency are obtained. The plasma jet enables control of the gas temperature and consequently influences the powder temperature.

The capabilities and the potential of the technology to obtain coatings on stainless steel and other substrates have been demonstrated using several material systems such as sintered carbides.

In order to evaluate the performance of the coating device, the coatings obtained were characterized chemically and physically. A physical model describing the complex processes taking place within the gun was developed. The model enables prediction of the main propelling gas and particle parameters, and in particular their acceleration and heating processes.

The project is performed in collaboration with groups from Tel-Aviv University and The Hebrew University, Jerusalem, under the sponsorship of the Israeli Ministry of Science. Sulzer-Metco, which is the world's leading industry in this field, contributes by supplying coating powders and some diagnostics services.

2. The ETCS Technology

The Electrothermal-Chemical Spray (ETCS) coating device is based on a conventional machine gun and munitions, and includes a pulsed-plasma ignition system. The munitions consist of a cartridge containing a selected propellant and the coating powder. Upon ignition, the drag force exerted by the combustion gases accelerates the powder particles towards the substrate where, subject to the particle's thermal and kinetic energy, it adheres to the topographical features. The buildup of the material thus deposited forms the coating.

A conventional gun cannot yield high quality coatings because the rise-time of the pressure is broad, and the combustion gas velocity field distribution is too wide. The Electrothermal-Chemical (ETC) Gun[1] works on a concept that overcomes these drawbacks. According to this method, the ignition and the combustion of the propellant are controlled by a pulsed-plasma ignition system consisting of a plasma jet provided by a confined electric discharge produced within an ablative capillary device[2,3]. Using this technique, a uniform coating can be obtained.

The employment of solid or liquid propellants combined with plasma augmentation has the advantages of: i) high powder velocity, ii) high throughput, iii) temperature control and iv) versatility.

The drag force exerted by the flowing gas on the moving particle controls the powder velocity. The drag force is given by [4, 5]:

$$F_D = C_D(R_e)\rho_g \frac{(V_g - V_P)^2}{8} \pi d_p^2 \qquad (1)$$

where $C_D(R_e)$ is the hydrodynamic drag coefficient of resistance and it is a function of the Reynolds number R_e; ρ_g and V_g are the propelling gas density and velocity, respectively; and V_P and d_P are the accelerated particles velocity and diameter, respectively. Expression 1 thus shows that an increase in gas velocity, gas density and acceleration time leads to high particle velocities. All these aspects are considered in our method.

Starting with solid or liquid propellants, considerably higher 'in-breech densities' are reached than those obtained

in HVOF or D-Gun. The prompt rise in pressure (~100 Mpa in ~ 200 μs) controlled by the dense, high-velocity plasma jet (7 - 10 km/s) ensures complete combustion of the propellant and results in high gas velocities. The barrel length controls the acceleration period. Theoretical predictions and preliminary experimental measurements indicate that in our setup, particle velocity higher than 1000 m/s can be reached.

Due to the high gas density, several grams of powder can be accelerated in a single shot. Therefore, we can reach throughputs that are three to five times higher than those obtained using competitive methods. For example, firing of 10 g powder per shot at a rhythm of 1 Hz results in a throughput of 36 kg/h.

The gas temperature is determined by interplay between the energy supplied by the propellant's combustion and the energy supplied by the plasma. The residence time of the powder in the gas can be minimized due to the high drag forces. Thus, most of the energy required to obtain good cohesion of the coating is recovered from the kinetic energy converted to heat during impact of the powder on the substrate. However, high gas temperature, and hence high particle temperature, can be obtained by increasing the rate and the total energy of plasma supplied.

The temperature affects the coating efficiency, defined as the proportion of powder sprayed that is deposited on the substrate. High yields (over 80% in certain cases) have been demonstrated for some sintered carbide coatings.

The coating sequence is pre-programmable and is set off-line. Thus, a sequence of one or more types of

munitions can be loaded and processed in one run. Every firing can be controlled independently. The amount and the type of the propellant, the powder material and the plasma parameters can be individually set for each coating element.

3. Coating Experiments

The experimental setup used in the coating experiments is shown in Figure 1. The setup is designed to give a single-shot coating splat. It consists of a standard gun tube, breech, cartridge and ignition system based on confined discharge plasma technology.

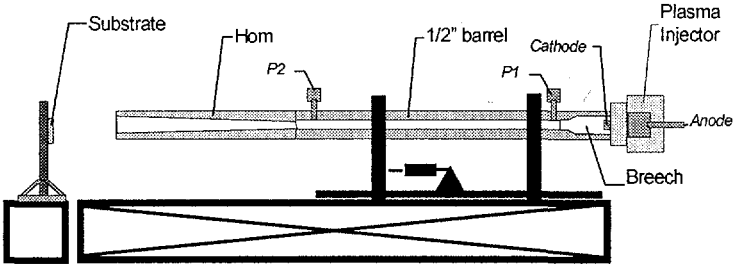

Fig. 1: The experimental setup

The gun is a standard 1/2" diameter, 1m-long gun tube. The 10 cm-long cartridge is inserted into the breech. The plasma injector is connected to the breech, with its cathode serving as the exit nozzle for the plasma jet. A detailed description of the plasma injector has been presented elsewhere [2].

A 57.5 cm-long horn is attached to the barrel. Its internal diameter tapers from the internal diameter of the barrel at one end, increasing to 40 mm at the horn muzzle. The gradual tapering of the horn smoothly reduces the pressure inside the barrel to that of the muzzle, maintaining the one-dimensional nature of the gases and the particle flow. The reduced pressure jump at the horn's exit decreases the radial drag and, in consequence, the radial velocity component. It decreases the turbulent flow of the

gases and the particles through the muzzle. This effect results in improved focusing of the powder and higher coating efficiency as compared with those obtained using conventional technologies. Two ports for pressure measurements are located along the barrel, the first (*P1*) at the breech exit and the second (*P2*) 10 cm from the muzzle of the straight barrel. The measured pressures are typically ~100 MPa at P1 and 10 - 20MPa at P2.

The distance between the exit muzzle of the coating device and the substrate to be coated is a coating variable that determines particle flight time and thus the extent of heat up and possible thermal degradation. The optimal distance varies from powder to powder as a function of the material sprayed and particle geometry. For sintered carbides, a typical spraying distance is 22 cm from the muzzle. Stainless steel discs (SS304), 5 mm thick and 60 mm in diameter, were used as substrates. The surface exposed to the powder was 50 mm in diameter. A polycarbonate holder with 5 cm inner- and 8 cm outer-diameter attached the substrate to be coated to the frame. Photographs of the substrate and the holder are shown in Figure 2.

WC-Co, Cr_3C_2-NiCr, Ta, Cr, Al_2O_3 and ZrO_2 powders were tested and an extensive report on the yields, efficiency, microstructural analysis and coating properties will be published soon. In this presentation just a few of the WC-Co and Cr_3C_2-NiCr experiments are presented.

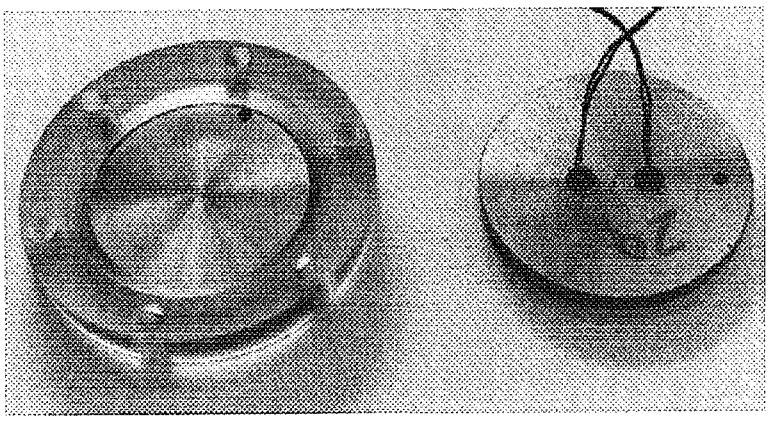

Fig. 2: Uncoated substrate and the holder

The carbide powder grain sizes ranged from 30 to 75 μm. A typical example of a SEM picture of aWC-Co grain is shown in Figure 3.

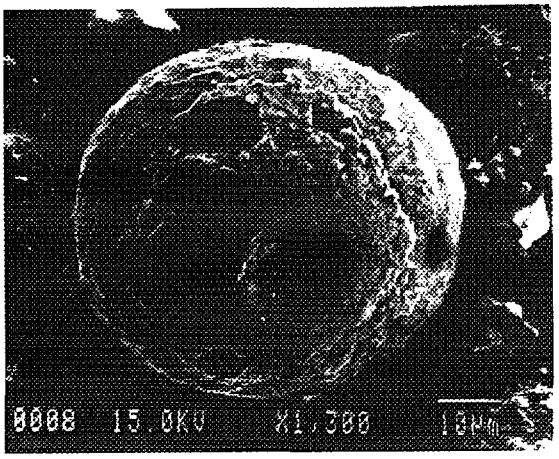

Fig. 3: SEM picture of tungsten carbide - cobalt (12%) powder grain (Sulzer-Metco 71NS)

The plasma injector (PI) was designed to have an Impedance in the range of 0.02-0.1Ω. The plasma parameters were evaluated using physical models [2,3], supported by experiments. Table 1 summarizes the plasma characteristics.

Pulse width	~150 μs
Pulse energy	1 – several kJ
Plasma temperature	~30,000°C
Plasma pressure	~1000 bar
Plasma velocity	~7000 m/s

Table 1 - Plasma characteristics

Several grams of conventional solid propellant were inserted in the cartridge case. In most of the WC/Co experiments, 6 g of propellant and 6 g of powder were used.

4. Results

4.1 Coating microstructure

Thick coatings (up to 260 μm) of WC/Co were formed in a single shot.

The micrographs in Figure 4 of a typical WC-Co coating have some distinctive features. Although the substrates were not pre-prepared by means such as sandblasting, degreasing, etc., good mechanical adhesion was obtained. This phenomenon can be explained by the deep penetration of the coating into the substrate as can be seen in Fig. 4b. The porosity in this case is approximately 1.5%.

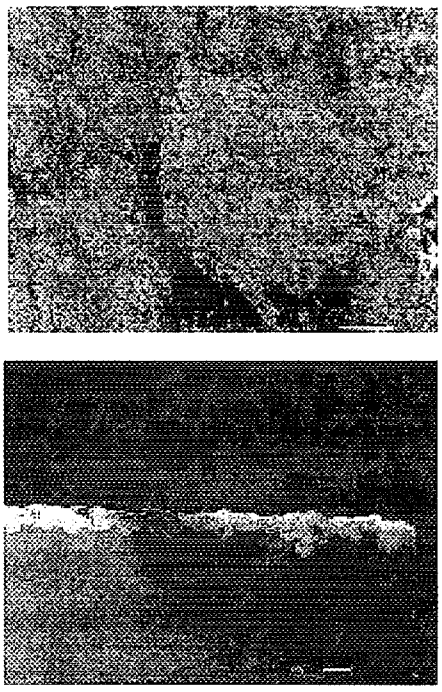

Fig. 4: SEM picture of a typical WC/Co coating at different magnifications. The bar shown represents 10μm in (a) and 100μm in (b).

The Vicker's microhardness values measured on the coatings had an average value of 1213 kg/mm^2 with a 300 g load and a standard deviation of 56.9 kg/mm^2.

Figure 5 shows a sample where a non-melted powder grain produced a crack in the coating. Since the theoretical model predicts relatively low average temperature of the powder particles the presence of a few non-melted particles may indicate the need to increase the plasma energy. It shows that the in-flight powder temperature distribution is not yet optimized in this experiment. However, a low in-flight temperature is of advantage in many cases, as it leads, to low evaporation losses of the powder and enables a high efficiency yield (over 80%). The existence of the uniform coating structure observed indicates that most of the powder particles are melted. The major part of the energy required to obtain the uniform coating structure is attributed to the conversion of the high particle kinetic energy to heat.

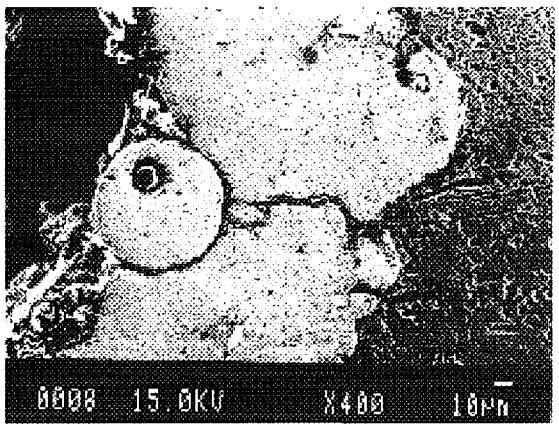

Fig. 5: SEM picture of cracked WC-Co coating due to non-melted grain impact

Figure 6 shows a coating of a Cr_3C_2 in NiCr matrix.

Typical coating thickness obtained was of the order of 150-200 µm and Vicker's microhardness values of 1210 kg/mm^2 with 300 g load were measured on the coating. The coating penetrated approximately 20 µm into the substrate. Again, the substrate was not pre-treated. The typical defects found in these coatings were vertical cracks that can be

attributed to thermal stress. The porosity in the sample was measured to be 1%.

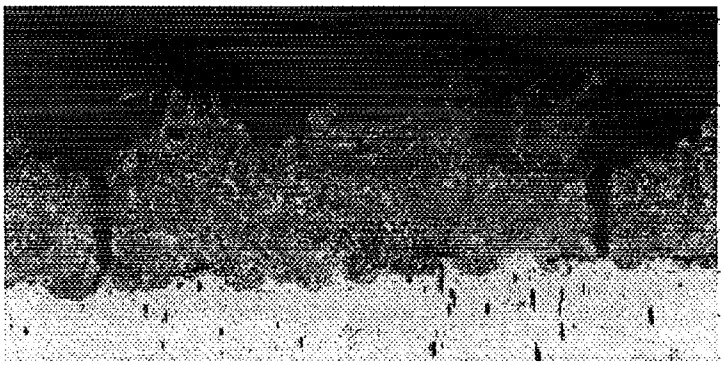

Fig. 6: Cr_3C_2-NiCr (Sulzer-Metco AMDRY 5260) on SS304 substrate

These initial results provide a proof-of-concept of the technology. However, as the number of controllable process parameters is high and as these parameters are interdependent, successful application of the technology for a specific material requires individual parameter optimization.

These optimizations can be assisted by model calculations based on theory, after which, the applicability of the theoretical model has to be verified experimentally.

5. Theory and Simulations

In order to gain further understanding of the coating process and to isolate the parameters that control its efficiency, extensive theoretical work was carried out. A new consistent physical model and simulation code was developed. From the practical point of view, our main goal in using the model developed was to predict the accelerated particle parameters that affect the coating quality and efficiency, such as particle velocity, temperature and phase at the device's muzzle. The model takes into account plasma injection, propellant ignition and combustion, gas flow, powder heating and acceleration along the barrel. The

scenario it describes is referred to as a two-phase reactive flow [6] and requires a rather complex solution.

The model describes the interaction between the plasma-gas mixture and the propellant (resulting in propellant ignition and combustion), the flow of the plasma-gas mixture and, finally, the powder particles' acceleration and heating. It contains two coupled sets of equations. The first set describes the so-called interior ballistic process [6] adapted to the specific conditions of the coating process, whereas the second set describes the accelerated particle characteristics within the framework of what is known as the 'dilute approximation' [4]. The 'dilute approximation' assumption means that the presence of the powder does not affect the gas-propellant interaction. Thus, there is only a 'one way' coupling between these two sets of equations.

5.1 The model equations

The interior ballistic process equations are based on a number of common assumptions published in the literature: see, for example, ref 6. The gas and solid phases are considered to occupy separate complementary regions and within each region the material may be treated as a homogeneous continuum. The flow of the heterogeneous mixture, composed of two interacting continua, is described by appropriately defined averages of flow parameters. The conservation equations based on these assumptions, together with the complementary constitutive laws, comprise the theoretical model. The following equations are used:

$$\frac{\partial}{\partial t}(\rho_1 r) + \frac{\partial}{\partial y}(\rho_1 r v) = \dot{m}_{21} + \dot{m}_{pl}(t, y) \qquad (2)$$

$$\frac{\partial}{\partial t}(\rho_2 R) + \frac{\partial}{\partial y}(\rho_2 R v) = -\dot{m}_{21} \tag{3}$$

$$\frac{\partial}{\partial t}(\rho_1 r v) + \frac{\partial}{\partial y}(\rho_1 r v^2) = -r\frac{\partial p}{\partial y} - f(v - V) + V\dot{m}_{21} + \frac{4}{3}\frac{\partial}{\partial y}\left(r\mu\frac{\partial v}{\partial y}\right) + P_{pl}(t, y) \tag{4}$$

$$\frac{\partial}{\partial t}(\rho_2 R V) + \frac{\partial}{\partial y}(\rho_2 R V^2) = -R\frac{\partial p}{\partial y} - f(v - V) - V\dot{m}_{21} - R\frac{\partial \tau}{\partial y} \tag{5}$$

$$\frac{\partial}{\partial t}\left[r\rho_1\left(\varepsilon + \frac{v^2}{2}\right)\right] + \frac{\partial}{\partial y}\left\{rv\left[p + \rho_1\left(\varepsilon + \frac{v^2}{2}\right)\right]\right\} = f(v - V)V - \dot{q}_{12} + \dot{m}_{21}\left(h_c + \frac{V^2}{2}\right) + S_{pl}(t, y) + \frac{v}{2}\frac{4}{3}\frac{\partial}{\partial y}\left(r\mu\frac{\partial v}{\partial y}\right) + \frac{4}{3}r\mu\left(\frac{\partial v}{\partial y}\right)^2 + \frac{\partial}{\partial y}\left(rK_g\frac{\partial T_1}{\partial y}\right) \tag{6}$$

$$\frac{\partial x}{\partial t} + V\frac{\partial x}{\partial y} = B \tag{7}$$

$$\frac{\partial H}{\partial t} + v\frac{\partial H}{\partial y} = \alpha_p q_s \tag{8}$$

where: ρ_1, ρ_2 are the gas and solid propellant densities, respectively, $\dot{m}_{21}$ and $\dot{m}_{pl}$ are the rates of burning gas and plasma production, respectively, r and $R \equiv 1 - r$ are the gas and solid volume fractions[6], respectively,. v and V are the gas and solid propellant velocities, respectively; τ is the intergranular stress; f is a factor proportional to the

interphase drag. P_{pl}, S_{pl} are the plasma source momentum and energy, respectively. Additional parameters describing relevant gas properties are: T_l - temperature, $\varepsilon \equiv C_v T_l$ - internal energy, p - pressure (given by the Abel-Nobel equation of state [6]), μ - viscosity coefficient, K_g - thermal conductivity. q_{12} is the density of the gas energy transferred to the solid propellant. Solid propellant properties: x - the linear regression of its surface during its combustion, B - its burning rate, q_s - energy flux incident on the solid propellant and H - thermal function [6] used to calculate the solid propellant surface temperature, and α_p its thermal diffusivity.

The particle equations derived and particle variables are as follows:

$$\frac{dV_\oplus}{dt} = \frac{3C_D\rho_1}{d_\oplus \rho_\oplus}(v - V_\oplus)\,|v - V_\oplus| \qquad (9)$$

$$\frac{dy_\oplus}{dt} = V_\oplus \qquad (10)$$

$$\frac{dy_\oplus}{dt} = \begin{cases} S_\oplus q_\oplus / m_\oplus C_\oplus & , \quad T_\oplus \neq T_{vap} \text{ and } T_\oplus \neq T_{melt} \\ 0 & , \quad T_\oplus \neq T_{vap} \text{ or } T_\oplus \neq T_{melt} \end{cases} \qquad (11)$$

$$\frac{dm_{vap\oplus}}{dt} = \begin{cases} 0 & , \quad T_\oplus < T_{vap} \\ S_\oplus q_\oplus / m_\oplus C_\oplus & , \quad T_\oplus = T_{vap} \end{cases} \qquad (12)$$

where: $V_\oplus, y_\oplus$ and $T_\oplus$ are the particle velocity, position and average temperature, respectively; $m_{vap\oplus}$ is the vapor phase mass; C_D is the drag coefficient (chosen to be 0.42); $d_\oplus, S_\oplus, \rho_\oplus$ and $m_\oplus$ are the particle diameter, surface area, density and total mass, respectively; $C_\oplus, \lambda_{vap}, T_{melt}$ and T_{vap}

are the particle specific heat (140 $J \cdot kg^{-1}K^{-1}$), vaporization heat ($4.33 \cdot 10^6$ J/kg), melting temperature (3269 K) and vaporization temperature (5773 K), respectively (The values in parentheses apply to tantalum particles).

5.2 Theoretical results

In Figures 7a-7c is shown the temporal evolution of a 30 μm diameter particle: (a) velocity, (b) temperature (compared with that of the propelling gas velocity and temperature) and (c) its mass loss.

As shown in Figure 7, the particle reaches a velocity of over 1200 m/s, which is considerably faster than the particle velocity obtained using alternative technologies presently employed in the coating industry. This velocity is very close to that of the gas (1400 m/s), a consequence of the strong drag force that acts on the particles because of the high gas density and velocity attained in our device.

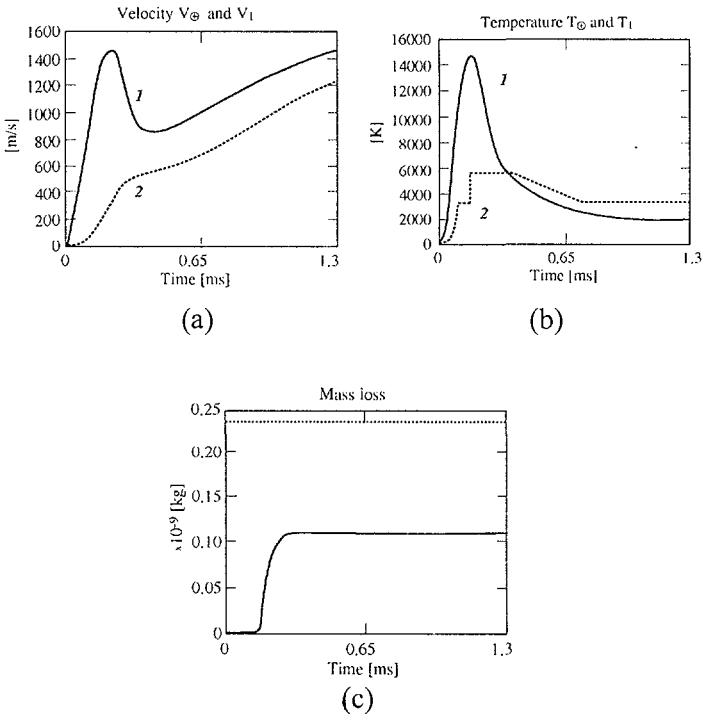

Fig. 7 - Temporal evolution of gas (1) and accelerated particle (2) parameters

As seen in Figure 7b, the gas and particle temperatures exhibit a complex behavior due to the various processes that the accelerated particle undergoes, which include heating, melting, and partial vaporization followed by cooling and re-solidification. As a consequence, the particle loses approximately 49% of its mass (Fig. 7c).

An example of the prediction capabilities is given in Figure 8, in which the velocity distribution for particles with seven different initial diameters (10, 20, 30, 40, 50, 60 and 70 μm, (lines 1-7), under the same ballistic conditions is shown.

It is notable, that the 10-μm-diameter particle (line 1) is vaporized and disappears before it reaches the muzzle. An important conclusion of the simulation is that the muzzle velocity of the particles as depicted in Figure 8 seems to be almost independent of the particles' initial diameter.

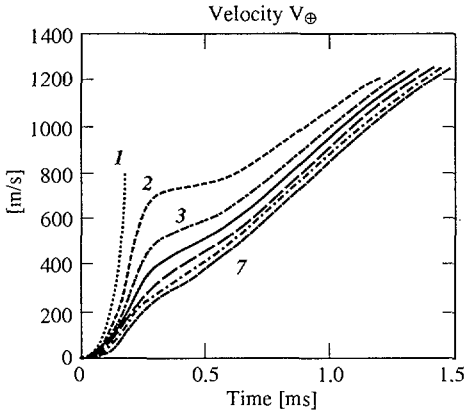

Fig. 8 - Velocity dependence on particle diameter

This is a very special and important feature of our device.

6. Model Validation Tests

6.1 The experimental setup

For the model validation tests, a powder-particles velocity measurement device was developed, and it is shown in Figure 9. Two parallel disks, 50 mm apart, are rotated by a 30,000 rpm motor. Two parallel masks, with 3 cm^2 opening area, reduce the amount of powder and gases that reaches the disks. In the front disk, eight holes with 1 cm diameter are evenly distributed on a circle of 15 cm diameter. A particle passing through a hole in the front disk is deposited on the second one. The displacement between the position of the deposited particles and that of the hole depends on the particles' time-of-flight between the disks and hence on the powder velocity.

A laser light that passes 16 notches marked on the disk's circumference, illuminates a photodiode. The photodiode signals are recorded and provide the average revolution speed between each pair of notches. The accuracy is better than 10% for velocities of ~1000 m/s.

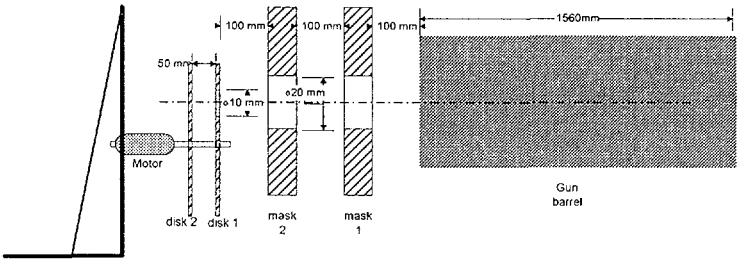

Fig. 9 - Velocity measurement device

The simulation predicted velocities of ~1000 m/s for tantalum powder; the observed velocity was 1045 m/s. For WC-Co powder lower velocities, of around 900 m/s are predicted. The measured value was 847 m/s. Both results are in good agreement with theory.

The length of coated arc on the front disk indicates that the powder cloud emerges from the device over a period of

~2 ms. The spread in time is due mainly to the different drag force applied on particles with different radii. As predicted by the model, all particles, even with different radius, finally reached almost the same velocity. Furthermore, the model predicts the 2 ms time distribution of the powder.

As the disks were revolving very fast only a thin, highly porous, coated layer was formed. Using SEM, individual particles were observed and their size measured and found to be consistent with the model predictions and theory.

The temporal pressure evolution measured at the breach and at the device muzzle and the theoretically predicted values were also found to be in a good agreement.

7. Final Remarks

A new coating technology based on the Electrothermal Gun concept is presented. The method enables the formation of high quality coatings at high throughput in a versatile off-line programmable manner.

Several powders were tested in a series of experiments. The coating's microstructure formed was characterized using optical microscopy and SEM. Work is in progress to measure the coating-substrate adhesion, hardness and wear resistance.

The experiments demonstrate that a wide range of parameters, such as the powder temperature, velocity, density, etc., can and should be controlled in order to achieve desired coating properties. Extensive theoretical work is being carried out in conjunction with proper experiments and coating characterization.

A model describing the new coating technology based on the Electrothermal Chemical Launcher concept has been developed and experimentally verified. Its predictions concerning some of the gas and particles characteristics are in good agreement with experimental measurements. The model indicates that a large number of parameters, such as the powder temperature, velocity, density, etc., must to be controlled and adjusted in order to generate particles having the desired properties for coating applications. Thus, the theoretical model can serve as a very useful tool for device and process optimization.

8. References

1. Morrison W.F., Wren G.P., and Oberle W.F., "Internal Ballistic Process in ETC Guns", Proceeding of the 13th Int. Symp. on Ballistics, Stockholm, Sweden, pp. 23-45 (1992).

2. Loeb A. and Kaplan Z., IEEE Trans. Magn. MAG-25, 342 (1989).

3. Zoler D., Saphir D., and Alimi R., "A Numerical Study of the Plasma Parameters Evolution in Ablative Capillary", J. Phys. D 27, 1423 (1994).

4. Rader J.R. and Geller A.S., Plasma Sources Sci. Technol. 3, 426 (1994).

5. Zoler D., Kaplan Z. and Ashkenazy J., Plasma Sources Sci. Technol. 5, 588 (1996).

6. Gough P. S., "XNOVA: An Express Version of the NOVA Code", PGA-TR-83-5, Portsmouth NH (1981).